Light focusing by slot Fabry–Perot photonic crystal nanoresonator on scanning tip

Lingyun Wang, Kazunori Hoshino, and Xiaojing Zhang*

Department of Biomedical Engineering, University of Texas at Austin, 10100 Burnet Road, Austin, Texas 78758, USA
**Corresponding author: john.zhang@engr.utexas.edu*

Received February 9, 2011; revised April 19, 2011; accepted April 24, 2011;
posted April 26, 2011 (Doc. ID 141616); published May 13, 2011

We numerically investigate the propagation of light through the photonic crystal (PhC) waveguide on low refraction index material for near-field light focusing at the visible wavelength (635 nm) by incorporating a center air slot and Fabry–Perot resonator on the scanning tip. Perturbations by water and substrate refraction index changes of the PhC are analyzed by the finite-difference time-domain method to show minimal impact on light confinement and throughput. Such a total dielectric probe tip design has great potential to complement the current widely used metal-coated optical-fiber-based light confinement probe. © 2011 Optical Society of America

OCIS codes: 130.5296, 130.2790.

We investigate the 2D subwavelength near field light focusing effect on low in-plane refraction index metamaterial. The subwavelength light source plays an important role in near-field scanning microscopy. By generating a light beam with spatial width far less than the wavelength, the imaging resolution goes beyond the diffraction limit and instead, is dominated by the light source size [1,2]. The low light throughput, due to mode mismatch, limits the applications of the optical-fiber-based probe. To increase the light transmission rate by plasmonic effects, many kinds of metal-based light enhancement structures have been proposed, such as the nanograting [3], superlens [4], bow-tie [5,6], and dipole antenna [7] around the tip aperture. However, there are two main drawbacks with the designs aforementioned, light absorption due to metal material at the visible wavelength [8] and the complicated manual assembly process. In this research a total dielectric photonic crystal (PhC)-based near-field light confinement probe embedded with a center air slot and Fabry–Perot (FP) nanoresonators is analyzed numerically at the operational wavelength of 635 nm. A typical low loss and low in-plane refraction index material is chosen to form the bulk material of the PhC, such as silicon nitride (Si_3N_4) with the refraction index of 2.02 for its compatibility with the planar silicon fabrication process.

The 2D PhC material is formed by arranging triangular air holes with radius $r = 0.3a$, where a is the lattice constant, through substrate material, as shown in Fig. 1(a). The minimum light confinement realized by the 2D PhC waveguide is around half wavelength through single line defect (W1) [9]. Other light processing devices, such as the slot waveguide and nanoresonator, are needed to further confine light to the subwavelength level. The dielectric air slot waveguide provides a low loss transport mechanism for TE-mode light, where the electric field is linearly polarized in the y direction [Fig. 1(a)] [10]. The light intensity peak concentrates in the air slot region with the full-width at half-maximum (FWHM) beam size proportional to that of the air slot due to the continuity boundary condition of the TE displacement field [11]. A slot PhC waveguide serves as the base structure by placing an air slot with size of $0.2a$ along the ΓK direction of the triangular lattice in the center of the waveguide defect. By setting $D_t = 1.48a$, which defines the distance between the bulk PhC air hole and the air slot [Fig. 1(a)], the PhC waveguide defect approximates a pseudo-W3 defect size. With the larger D_t, the new design relaxes the critical fabrication requirement, as compared to the W1 slot PhC waveguide [12] design. So the nanoresonator air holes later on can be placed around the center defect

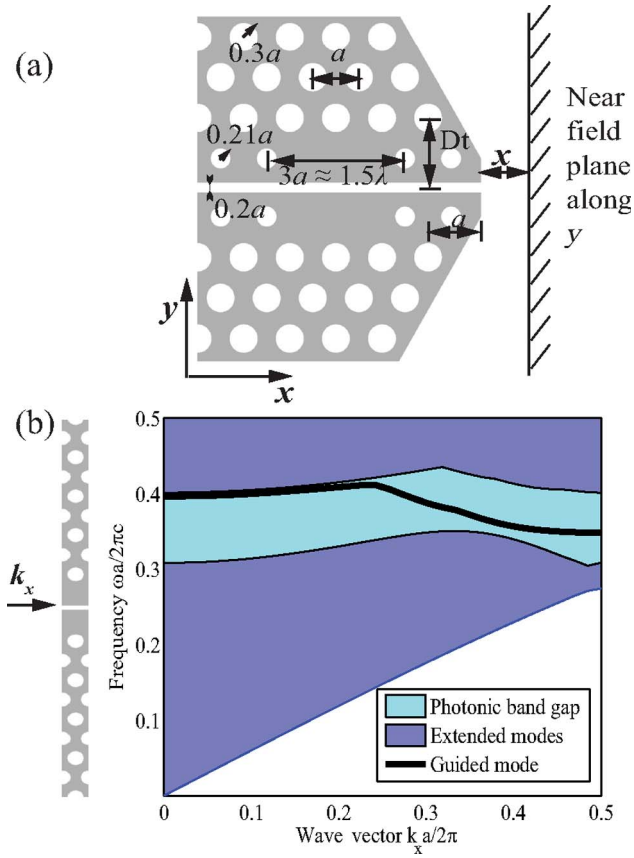

Fig. 1. (Color online) Design of 2D slot FP PhC nanoresonator based probe on triangular air holes lattice. (a) Probe design illustrated in terms of lattice constant a where $D_t = 1.48a$. White and gray colors represent air and low refraction index material, respectively. (b) Projected band structure along the x direction of the slot PhC waveguide without nanoresonator formed by air hole radius of $0.3a$ (refraction index $n = 2.02$) for TE mode with the super cell lattice shown on the left.

with ease without destructing the overall device features. The photonic band diagram, calculated by plane wave expansion method using a supercell, as indicated at the left of Fig. 1(b), yields the guided mode, under which the optimal lattice size can be derived [13]. A guided mode in the gap center is chosen near the first Brillouin zone edge for the device design, because the magnetic field ($\boldsymbol{H}_z$) distribution pattern is symmetric in the $\boldsymbol{y}$ direction for the TE mode, which excites symmetrically across the slot and provides light localization in the slot region. At the chosen guided mode, there is $\frac{\omega}{2\pi c} = 0.356$, where c is the speed of light in free space. For wavelength $\lambda_0 = 635\,\text{nm}$, the lattice constant a is derived as $a = 0.356\,\lambda_0 = 226\,\text{nm}$, and the slot size $0.2a$ equals 45 nm, which decides the minimum feature size of the device. The probe tip is shaped by removing the bulk PhC air holes along the $\boldsymbol{\Gamma K}$ direction, forming a 120° cone probe body. The probe body side cutting edges are aligned with the next line bulk PhC air hole edges. The final flat aperture surface is aligned in the $\boldsymbol{y}$ direction positioned $0.5a$ in the $\boldsymbol{x}$ direction away from the nearest mirror air holes.

The probe is modeled by the finite-difference time-domain (FDTD) method (Fig. 2) with a grid size of 2 nm and a perfectly matched layer thickness of 1 μm surrounding the four boundaries of the calculation domain to reduce the reflections errors [14]. A TE light source with a Gaussian profile launches in a rectangular ridged waveguide with the same size of the PhC center defect. The FDTD calculation is converged after turning on the continuous source for time that allows the waves to propagate through the whole structure for at least 20 times and reaching a steady state before collecting the data at the monitoring planes. Performance of the probe is assessed in the near-field distance ranging from 0 to 30 nm with a step size of 2 nm. For straight slot PhC waveguide termination, there are strong reflections back to the probe body due to the PhC–air boundary, and the center peak inside the slot also splits into two strong side lobes [Fig. 2(c)], which is not fit for near-field light confinement purposes. In order to make a near-field light confinement tip, FP resonator, formed by two smaller mirror air holes anchored in the bulk lattice position with radius of $0.7r$ along the sides of the air slot [Fig. 1(a)], is incorporated in the slotted PhC waveguide to enhance the light throughput and block the strong side lobes to make it a single peak probe at the near field. The cavity size of the FP resonator is around 1.5λ (λ is the wavelength in the substrate medium) by isolating mirroring holes with distance of $3a$ to form a constructive interference [15]. As the distance from the tip aperture increases, the center light intensity decreases but the single peak is kept all the way to a 30 nm near-field distance. At a 10 nm near-field distance, the FWHM of the light beam is 87.8 nm, which is about $\lambda/7$ with peak intensity of 7.6%, twice of that of the one without the resonator (all the light intensity is normalized to the light source intensity peak).

Because the near-field light confinement is in the sub-wavelength level and very close to the tip aperture, it is necessary to study the light distribution changes due to the impacts from both the refraction index changes in the PhC substrate and the higher refraction index object in the near field. A flat water medium with refraction index of 1.33 is placed 10 nm away from the tip aperture [Fig. 3(a)], because the normal near distance control for the near-field imaging system is most accurate in the sub-10 nm range [16]. This kind of configuration mimics the scenario of biological imaging applications, because most cells have high water content, with only a 4 to 5 nm lipid bilayer cell membrane [17]. Two monitoring planes at the near field of 5 and 15 nm along the y direction are chosen to assess the probe near-field focusing capabilities in terms of the FWHM and center peak intensity of the light beam as functions of the PhC substrate refraction index ranging from 1.97 to 2.07, which is about ±2.5% from the typical Si_3N_4 index ($n = 2.02$) [Figs. 3(b) and 3(c)].

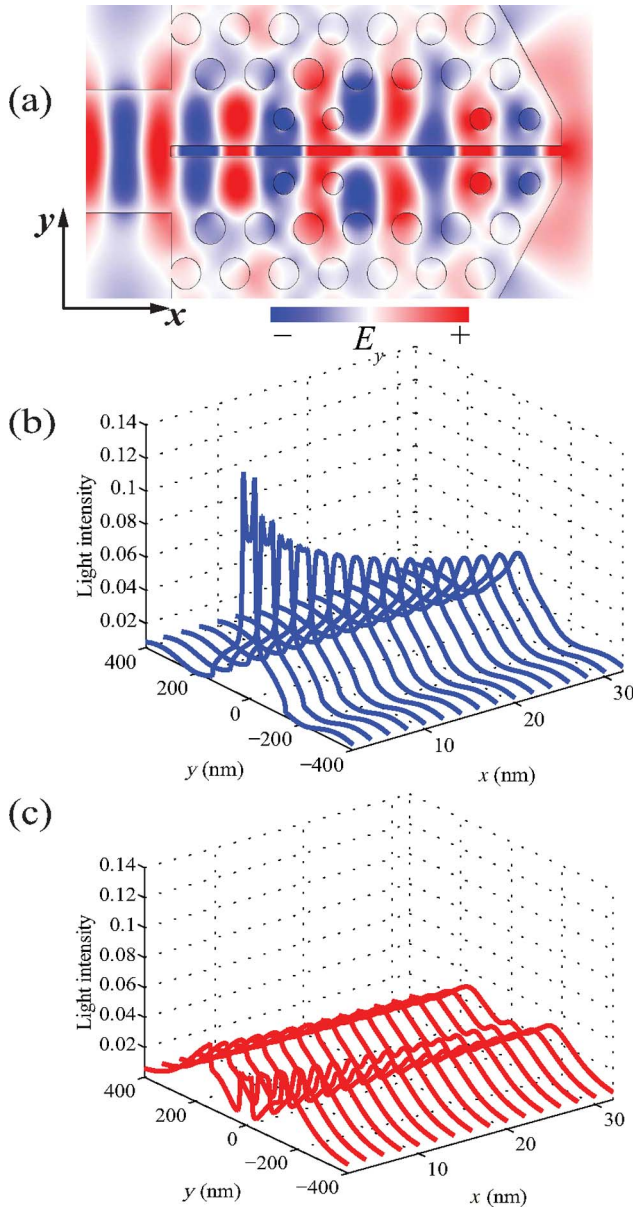

Fig. 2. (Color online) FDTD analysis of light confinement on probe without any perturbations. (a) Surface plot of electric field E_y distribution pattern of the slot PhC FP probe with bulk PhC index $n = 2.02$. (b) Light intensity distribution at near field of the probe, where $\boldsymbol{x}$ is the near field distance from the tip aperture, ranging from 0 to 30 nm with 2 nm step. (c) Light distribution at near field of the probe without embedding nanoresonators.

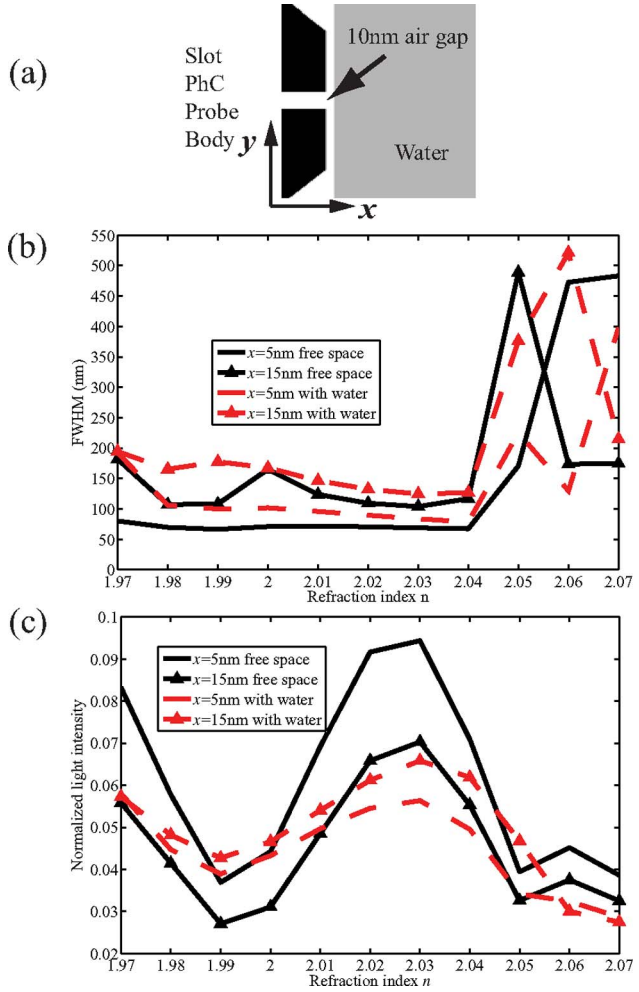

Fig. 3. (Color online) Perturbations on light confinement. (a) Illustration of water medium in the near field of the probe tip with 10 nm air gap between tip and water film. (b) FWHM plot of the light center peak and (c) normalized center peak intensity in 5 and 15 nm near-field distance with PhC bulk refraction index varying from 1.97 to 2.07 for both free space case and water film in the near-field case.

Perturbation from the refraction index change of the bulk PhC causes beam splitting for a refraction index greater than 2.04. For an index ranging from 1.97 to 2.04, the FWHM is always less than 200 nm for all scenarios, and due to the impact from the water medium in the near field, the FWHM increases slightly about 30 nm in the center index range from 2.00 to 2.04. The "concave lens" effect, due to the near-field distance between the probe tip and water film, causes the spreading of the wave front that enlarges the beam size in the near field.

In conclusion, the near-field focusing effects of the slot FP PhC nanoresonator of low in-plane index contrast and a pure dielectric material can provide subwavelength light confinement at the visible wavelength of 635 nm. The perturbation changes in the PhC substrate dielectric property cause beam splitting for refraction indices higher than 2.04. Perturbation from the water medium causes slight beam spreading, but it is still under the subwavelength range.

References

1. E. H. Synge, Philosoph. Mag. **6**, 356 (1928).
2. A. Lewis, H. Taha, A. Strinkovski, A. Manevitch, A. Khatchatouriants, R. Dekhter, and E. Ammann, Nat. Biotechnol. **21**, 1378 (2003).
3. H. J. Lezec, A. Degiron, E. Devaux, R. A. Linke, L. Martin-Moreno, F. J. Garcia-Vidal, and T. W. Ebbesen, Science **297**, 820 (2002).
4. N. Fang, H. Lee, C. Sun, and X. Zhang, Science **308**, 534 (2005).
5. S. Kim, J. Jin, Y.-J. Kim, I.-Y. Park, Y. Kim, and S.-W. Kim, Nature **453**, 757 (2008).
6. K. Ishihara, K. Ohashi, T. Ikari, H. Minamide, H. Yokoyama, J.-I. Shikata, and H. Ito, Appl. Phys. Lett. **89**, 201120 (2006).
7. T. H. Taminiau, F. D. Stefani, F. B. Segerink, and N. F. van Hulst, Nat. Photon. **2**, 234 (2008).
8. P. G. Gucciardi, M. Colocci, M. Labardi, and M. Allegrini, Appl. Phys. Lett. **75**, 3408 (1999).
9. J. D. Joannopoulos, S. G. Johnson, J. N. Winn, and R. D. Meade, *Photonic Crystals: Molding the Flow of Light*, 2nd ed. (Princeton U. Press, 2008).
10. C. A. Barrios, B. Sanchez, K. B. Gylfason, A. Griol, H. Sohlstrm, M. Holgado, and R. Casquel, Opt. Express **15**, 6846 (2007).
11. V. R. Almeida, Q. Xu, C. A. Barrios, and M. Lipson, Opt. Lett. **29**, 1209 (2004).
12. L. Wang, K. Hoshino, and X. Zhang, Proc. SPIE **7729**, 77291M (2010).
13. S. G. Johnson and J. D. Joannopoulos, Opt. Express **8**, 173 (2001).
14. A. F. Oskooi, D. Roundy, M. Ibanescu, P. Bermel, J. D. Joannopoulos, and S. G. Johnson, Comput. Phys. Commun. **181**, 687 (2010).
15. A. V. Kudryashov and H. Weber, *Laser Resonators: Novel Design and Development* (SPIE 1999).
16. E. Betzig, P. Finn, and J. Weiner, Appl. Phys. Lett. **60**, 2484 (1992).
17. P. W. Kuchel and G. B. Ralston, *Theory and Problems of Biochemistry*, 2nd ed. (McGraw-Hill 1988).